Fluorescent Probes Hot Paper

Zitierweise:
Internationale Ausgabe: doi.org/10.1002/anie.202101190
Deutsche Ausgabe: doi.org/10.1002/ange.202101190

Rational Design of a Highly Selective Near-Infrared Two-Photon Fluorogenic Probe for Imaging Orthotopic Hepatocellular Carcinoma Chemotherapy

Xiaofeng Wu[+], Rui Wang[+], Sujie Qi, Nahyun Kwon, Jingjing Han, Heejeong Kim, Haidong Li, Fabiao Yu and Juyoung Yoon**

Abstract: *Selective fluorescence imaging of biomarkers in vivo and in situ for evaluating orthotopic hepatocellular carcinoma (HCC) chemotherapy remains a great challenge due to current imaging agents suffering from the potential interferences of other hydrolases. Herein, we observed that carbamate unit showed a high selectivity toward the HCC-related biomarker carboxylesterase (CE) for evaluation of treatment. A near-infrared two-photon fluorescent probe was developed to not only specially image CE activity in vivo and in situ but also target orthotopic liver tumor after systemic administration. The in vivo signals of the probe correlate well with tumor apoptosis, making it possible to evaluate the status of treatment. The probe enables the imaging of CE activity in situ with a high-resolution three-dimensional view for the first time. This study may promote advances in optical imaging approaches for precise imaging-guided diagnosis of HCC in situ and its evaluation of treatment.*

Introduction

Fluorescence imaging has been emerging as a powerful method for realizing the selective imaging of enzyme activity in vivo for accurate diagnosis, and therapy of cancer and evaluations of corresponding drug treatments because of its unique advantages, including good sensitivity and selectivity, in situ and/or real-time detection, high spatiotemporal resolution and noninvasive monitoring ability in living systems.[1] However, due to strong intrinsic light scattering in tissue, spatial resolution and penetration are rapidly compromised in imaging in vivo with depth. Near-infrared (NIR) two-photon (TP) fluorescence imaging is a promising tool for in vivo imaging of enzyme activity with decreased autofluorescence, high tissue penetration and resolution.[2]

Hepatocellular carcinoma (HCC) is a highly aggressive liver malignancy and a major cause of cancer-associated death.[3] An effective method is still urgently required for precisely diagnosing the condition of liver and evaluating drug treatments. In medicine, biomarkers can be tested in blood, tissue and body fluids as sign reflecting the normal or abnormal conditions, allowing the evaluating of individual treatment for cancer and detections of cancer at early stages.[4] Thus, given that carboxylesterase (CE) is an important biomarker of HCC, a selective and sensitive fluorescent probe for testing CE levels in vivo may be an effective tool for indicating the severity or presence of liver conditions.[5] As a mainstream approach for biomarker detection, the specificity of serum assays may be impaired due to biomarkers or interference in the multiple organs or tissues in addition to the disease lesions.[6] Biomarker analysis at a specific origin can more accurately reflect the real condition of the liver under drug treatment. In addition, an ideal method for testing biomarkers ought to have higher selectivity.[4b]

Thus, an activatable and highly selective NIR TP fluorescent probe for localizing spatially and elevating CE levels in the original hepatic organ is rather important and meaningful for better accurate imaging-guided diagnosis of the orthotopic HCC and its evaluation of treatments. As an indispensable element of fluorescent probes, recognition moieties are extremely responsible for selective and sensitive interactions with enzymes of interest.[7] However, currently, ester bonds such as acetyl units are still employed as a main recognition moiety for constructing fluorescent probes for CE activity besides butyrylcholinesterase (BChE) and acetylcholinesterase (AChE), resulting in potential mutual interferences.[8] This may seriously compromise the accurate measurement of CE activity in vivo and in situ. This great challenge encourages us to engineer a selective recognition moiety for constructing a NIR TP fluorescent probe for imaging the CE. Fortunately, we noticed that rivastigmine and physostigmine (commercial inhibitors of BChE and AChE) contain carbamate moieties that can function to inhibit the activity of BChE and AChE (Scheme 1 A).[9] However, irinotecan (CPT-11) as a precursor of an anticancer drug containing a carbamate unit could be a substrate catalyzed by CE to release anticancer SN38 (Scheme 1 A and Figure S1).[10] This indicates that compounds containing carbamate units

[*] Dr. X. Wu,[+] S. Qi, Dr. N. Kwon, J. Han, H. Kim, Dr. H. Li, Prof. Dr. J. Yoon
Department of Chemistry and Nanoscience, Ewha Womans University
Seoul 03706 (Republic of Korea)
E-Mail: jyoon@ewha.ac.kr
Dr. R. Wang,[+] Prof. Dr. F. Yu
Key Laboratory of Emergency and Trauma, Ministry of Education, Key Laboratory of Hainan Trauma and Disaster Rescue, The First Affiliated Hospital of Hainan Medical University, Institute of Functional Materials and Molecular Imaging, College of Emergency and Trauma, Hainan Medical University
Haikou 571199 (China)
E-Mail: yufabiao@hainmc.edu.cn
[+] These authors contributed equally to this work.
Supporting information and the ORCID identification number(s) for the author(s) of this article can be found under: https://doi.org/10.1002/anie.202101190.

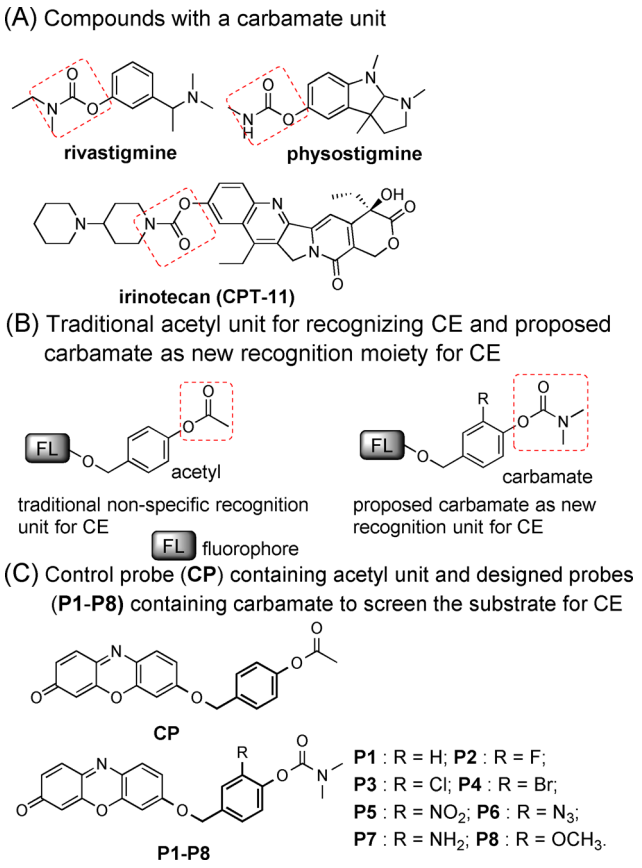

Scheme 1. Illustration of the carbamate proposed as a new specific recognition moiety for CE. A) Compounds with a carbamate unit. B) Traditional acetyl unit for CE and the carbamate proposed as a new specific recognition unit for CE. C) Control probe (**CP**) and probes (**P1**–**P8**) designed to screen substrates with the best selectivity for CE.

may selectively react with CE but simultaneously inhibit the activity of BChE and AChE, inspiring us to employ carbamate as a specific recognition unit for CE that can avoid potential interference from AChE and BChE.

In this study, with these concerns and inspirations in mind, we designed and synthesized a series of compounds containing carbamate for screening the substrate with the best selectivity for CE over BChE and AChE. To decrease the steric hindrance between the signaling unit and active site of enzyme,[11] these compounds were prepared using substituted self-immolative linker as a bridge between the signaling unit (resorufin) and carbamate moiety (Schemes 1B and C).[12] The detection mechanism is based on hydrolysis by CE, followed by 1,6-rearrangement elimination to afford free resorufin (Figure S2). Based on the screened recognition moiety of substrate with the best selectivity (**P3** of Scheme 1c), we further developed a light up NIR TP fluorescent probe (**DCM-Cl-CE**, Scheme 2).[13] As expected, this NIR TP fluorescent probe also displays excellent selectivity for CE over BChE and AChE, and shows a new broad emission band in the NIR region. Moreover, this probe accurately enables monitoring the change in CE activity in cells treated with anticancer drugs. Meanwhile, this conversely allows for in vivo selective imaging of CE activity in orthotopic liver tumor

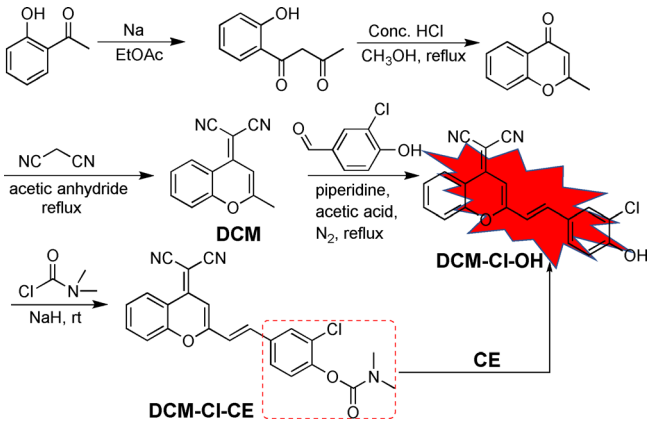

Scheme 2. Synthesis of the NIR TP fluorescent probe (**DCM-Cl-CE**) for CE and its reaction mechanism with CE.

mice treated with anticancer drug, reflecting real conditions of HCC. Importantly, to the best of our knowledge, this is the first light up NIR TP fluorescent probe for in vivo and in situ tracking of CE activity using high-resolution three-dimensional (3D) fluorescence imaging, possibly allowing for image-guided diagnosis, evaluation of treatment and surgical resection of orthotopic hepatocellular tumors.

Results and Discussion

Design and Syntheses of CP, P1-P8 and DCM-Cl-CE

A control probe (**CP**) containing an acetyl moiety was synthesized for comparison. **P1**–**P8** were prepared using the self-immolative linker with different substituted groups (hydrogen, fluoride, chloride, bromo, nitro, azide, amine and methoxyl groups) to combine the carbamate unit with resorufin (Schemes 1B and 1C). The substituted units could also be used to tune the selectivity toward CE over BChE and AChE. These compounds were used as substrates to screen recognition moiety with the best selectivity and reactivity for CE activity. To make the probe suitable for imaging CE in vivo, based on the specific recognition moiety of **P3** presenting the best selectivity and reactivity toward CE, we designed and prepared an NIR ($\lambda_{em} > 650$ nm) TP fluorescent probe (**DCM-Cl-CE**, Scheme 2). All the detailed synthetic steps, characterizations and reaction mechanisms are shown in Scheme 1 and Scheme 2, and the Supporting Information.

Screening Recognition Moiety with the Optimal Selectivity for CE

We first checked the selectivity of **CP** and **P1**–**P8** toward CE, BChE and AChE, respectively. As shown in Figures 1A and S3, under the same conditions, **CP** has almost the same response toward CE as AChE and BChE, indicating that this traditional recognition moiety of acetyl unit is not selective for CE and a fluorescent probe with acetyl unit for CE is interfered by BChE and AChE. As shown in Figures 1B–D,

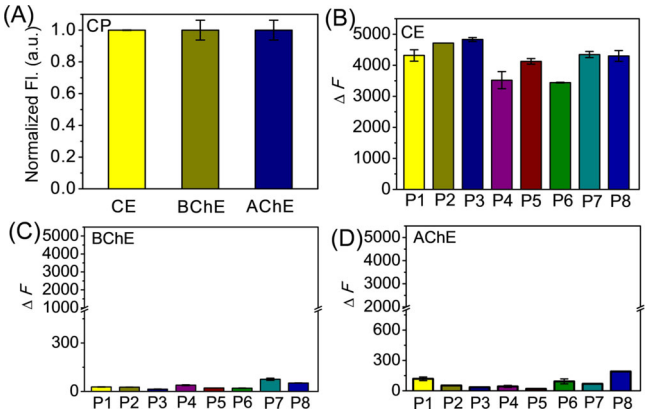

Figure 1. A) Normalized fluorescence intensity of **CP** (5 μM) reacting with CE, BChE and AChE (1 U mL^{-1}) for 0.5 h at 37 °C in PBS buffer (pH 7.4), respectively. Fluorescence response of **P1**–**P8** (5 μM) toward B) CE (1 U mL^{-1}), C) BChE (1 U mL^{-1}) and D) AChE (1 U mL^{-1}) for 5 h at 37 °C in PBS buffer (pH 7.4), respectively. ΔF is the fluorescence intensity difference after and before the reaction. The results are expressed as the mean ± SD ($n = 3$). $\lambda_{ex}/_{em} = 550/582$ nm.

S3 and S4, **P1**–**P8** all produced better response toward CE but had almost no any response to BChE and AchE. The ratios of fluorescence changes from reactions of probes with CE, BChE and AChE were termed R1 and R2, respectively, further clearly indicating the selectivity of CE over BChE and AChE. Table 1 shows that the values of R1 and R2 for CP are 1.03 and 1.0, respectively, again clearly demonstrating that the acetyl unit has no difference in response to CE, BChE and AChE. However, the values of R1 vary from 48.75 to 338.3, showing that **P1**–**P8** all have better selectivity for CE over BChE. **P3** has the best selectivity ($R1 = 338.3$) while **P6** displays the worst selectivity. In addition, for the selectivity of CE over AChE, the R2 values for **P1**–**P8** ranging from 22.5 to 421 also indicated that **P1**–**P8** all have better selectivity toward CE than AChE, among of which **P5** and **P3** have relatively better selectivity. Altogether, **P3** shows a better recognition moiety for CE than BChE and AChE. All the above data show that our design using carbamate to replace the acetyl unit as a selective recognition moiety for CE is rational and effective.

Tabelle 1: Selectivity of CE over BChE and AChE.

Compd.	CE[a]	BChE[a]	AChE[a]	R1[b]	R2[c]
CP	4833	4708	4835	1.03	1.0
P1	4371	28.1	118.9	153.6	36.6
P2	4716	26.56	52.41	177.6	90.0
P3	4831	14.28	32.7	338.3	148.0
P4	3520	38.85	44.06	90.6	79.9
P5	4126	21.53	9.8	191.6	421.0
P6	3442	70.6	92.97	48.75	37.0
P7	4346	75.44	70	57.6	62.1
P8	4299	52.3	191.1	82.2	22.5

[a] Fluorescence intensity difference (ΔF) of probes (5 μM) with CE, BChE and AChE (1 U mL^{-1}), respectively, after and before reaction. [b] R1 = (ΔF of CE)/(ΔF of BChE). [c] R2 = (ΔF of CE)/(ΔF of AChE), indicating the selectivity of CE over BChE and AChE. All were measured in PBS solution (7.4).

Selectivity of DCM-Cl-CE toward CE over BChE and AChE

As mentioned above, to further make it possible to image CE activity in vivo, an NIR TP fluorescent probe (**DCM-Cl-CE**) was prepared based on the best selective recognition unit of **P3** (Scheme 2). The selectivity of **DCM-Cl-CE** with CE, BChE and AChE was also first investigated. Upon titration with 1 U mL^{-1} of CE, BChE and AChE, as shown in Figures 2A and S5, the reaction of **DCM-Cl-CE** with CE produced a significant enhancement while the reactions of **DCM-Cl-CE** with BChE and AChE did not generate any fluorescence. In addition, no fluorescence peak was observed for **DCM-Cl-CE** reacting with BChE and AChE, indicating that almost no reaction occurred. This shows that carbamate is an excellent recognition moiety for CE, and **DCM-Cl-CE** is a highly selective NIR TP fluorescent probe for the detection of CE activity in vivo.

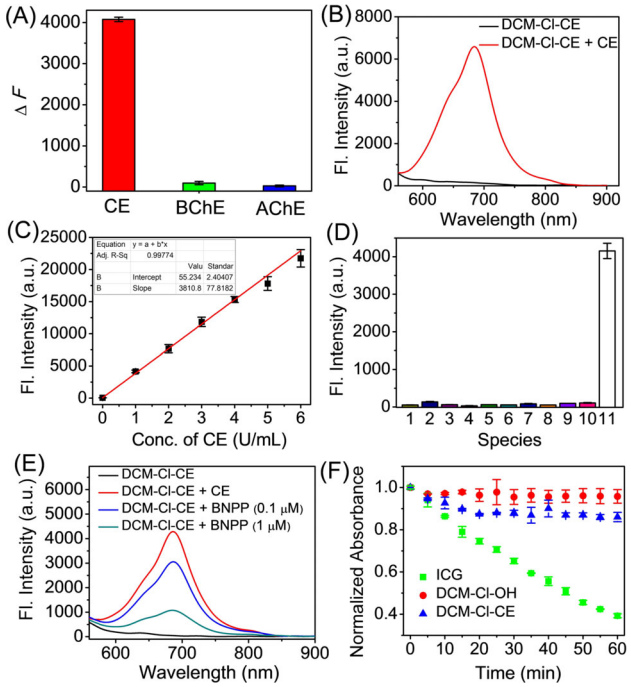

Figure 2. In vitro properties of **DCM-Cl-CE**. A) Fluorescence response of **DCM-Cl-CE** toward CE, BChE and AChE (1 U mL^{-1}). B) Fluorescence spectra of **DCM-Cl-CE** (5 μM) in the absence and presence of CE (1 U mL^{-1}). C) Linear relationship between the fluorescence intensity and CE concentration (0–6 U mL^{-1}) for 5 h at 37 °C. D) Fluorescence response of **DCM-Cl-CE** (5 μM) to various enzymes, including (1) the blank, (2) β-glucosidases (10 U mL^{-1}), (3) xanthine oxidase (10 mU mL^{-1}), (4) tyrosinase (10 U mL^{-1}), (5) ALP (10 U mL^{-1}), (6) MAO-A (10 μg mL^{-1}), (7) MAO-B (10 μg mL^{-1}), (8) trypsin (10 μg mL^{-1}), (9) HSA (10 μM), (10) BSA (10 μM) and (11) CE (1 U mL^{-1}). E) Inhibitory activity of **DCM-Cl-CE** against BNPP under different conditions. F) Photostability of **DCM-Cl-CE**, **DCM-Cl-OH** and ICG in PBS detected via absorbance spectra. The samples (all at 5 μM) were continuously irradiated by a light source (25 mW cm^{-2}).

Spectroscopic Properties of DCM-Cl-CE and Its Responses to CE

To test the validity of this probe, the spectroscopic properties of **DCM-Cl-CE** were investigated in physiological

buffer. **DCM-Cl-CE** itself shows a peak at 400 nm while upon reaction with CE, the absorbance shifts to approximately 540 nm (Figure S6), which is roughly consistent with the absorbance peak of **DCM-Cl-OH** (Figure S7). The color ranges from yellowish to rose red, making it favorable for colorimetric detection using the naked eye (Figure S6). As expected, when excited at 540 nm, an NIR fluorescence signal at 685 nm was observed fully matching the emission wavelength of **DCM-Cl-OH** (Figures 2B and S8). Time-dependent experiments revealed that after 5 h, 83-fold fluorescence enhancement could be found at 685 nm (Figure S9), benefiting the sensitive detection of CE. The fluorescence intensity almost reached a maximum with buffer solution incubated at 37 °C (Figure S10). The plot between the concentration of **DCM-Cl-CE** and the emission intensity is displayed, and good linearity was obtained at concentrations of 0–6 $U\,mL^{-1}$. The linear regression equation is $F = 3381 \times [\text{activity of CE}] + 55.2$, with a correlation coefficient of 0.998. The limit of detection (3σ/slope) is 0.013 $U\,mL^{-1}$,[12] also showing sensitive detection of CE (Figures 2C and S11). The Michaelis–Menten constant (K_m) and the catalytic constant (k_{cat}) of CE toward **DCM-Cl-CE** were also measured to be 0.21 μM and 0.91 s^{-1}, respectively (Figure S12). The catalytic efficiency (k_{cat}/K_m) of CE for **DCM-Cl-CE** was calculated to be $4.52 \times 10^6\ M^{-1}s^{-1}$. These data indicated that CE displays high affinity and effective cleavage toward **DCM-Cl-CE**. The maximum TP absorption cross section (δ) was also determined to be 24.1 GM at 830 nm (Figure S13), implying that CE could be imaged by **DCM-Cl-CE** with a TP microscope.

To investigate the interference, the reaction of **DCM-Cl-CE** with various species was performed, including enzymes [β-glucosidases, xanthine oxidase, tyrosinase, alkaline phosphatase (ALP), monoamine oxidase A/B (MAO-A/B), and trypsin], human serum albumin (HSA), bovine serum albumin (BSA), several inorganic salts, glucose, vitamin, some amino acids, glutathione, urea and various reactive oxygen species (Figures 2D, S14 and S15). However, only when treated with CE was the strongest and most distinct fluorescence enhancement observed. These results indicate the super excellent selectivity of **DCM-Cl-CE** toward other competitive species, which is required for selective and accurate detection under complex biosystems.

Moreover, an inhibitory experiment was performed to demonstrate that the reaction site was cleaved by CE. The effect of an inhibitor of CE, bis(4-nitrophenyl)phosphate (BNPP) was examined.[14] As shown in Figure 2E and S16, compared to the group (**DCM-Cl-CE** + CE), with increasing concentrations of BNPP, the fluorescence intensity decreased dramatically, indicating that the fluorescence change of the reaction indeed arose from CE-catalytic hydrolysis.

Stabilities of DCM-Cl-CE and DCM-Cl-OH

Their high stability benefits **DCM-Cl-CE** and **DCM-Cl-OH** in performing in vivo long-term tracking of enzyme activity in preclinical applications. The photostability of **DCM-Cl-CE** and **DCM-Cl-OH** was estimated based on time-course absorbance measurements under continuous irradiation by a light source with a power of 25 $mW\,cm^{-2}$ in aqueous solution. The clinically approved NIR dye indocyanine green (ICG) was chosen as the control compound.[15] As shown in Figures 2F and S17, after continuous exposure to light for 1 h, an almost 61 % decrease in absorbance indicated that 39 % of ICG was left. However, almost 100 % **DCM-Cl-OH** and 90 % **DCM-Cl-CE** remained under the same conditions. The photostability of both **DCM-Cl-OH** and **DCM-Cl-CE** is better than that of ICG. In addition, the effect of the temperature on the thermal stability was also investigated. Different temperatures (25, 30, 37 and 42 °C) and long-term incubation at 37 °C also had almost no effect on the stability of **DCM-Cl-CE** and **DCM-Cl-OH** (Figures S10, S18 and S19). These data show that high photo- and thermal stabilities are highly desirable for long-term tracking and bioimaging of CE activity in vivo.

pH Profiles of DCM-Cl-CE and DCM-Cl-OH

The pH is an important factor that has great effect on the photophysical properties of probes. Consequently, the pH-dependent fluorescence emission profiles were evaluated. There was negligible change in fluorescence emission at 685 nm for **DCM-Cl-CE** in pH range from 4.0–11.0. Upon titration with CE, fluorescence intensity enhancement was generated, and the strongest fluorescence intensity could be observed at pH 7.4, making **DCM-Cl-CE** desirable for the detection of CE activity under physiological conditions (Figure S20). Besides, the hydrolytic product of **DCM-Cl-CE**, that is **DCM-Cl-OH** was found its p*K*a is calculated to be 7.18 (Figures S21 and S22), also allowing **DCM-Cl-CE** to working better under the physiological conditions of living systems.

Comparison of CE Activity within Human Liver Cancer Cells and Normal Liver Cells

The high selectivity, sensitivity and stability of **DCM-Cl-CE** make it possible to image CE activity in living cells. The HepG2 cell line (human liver cancer cell) and LO2 cell line (human normal liver cell) were chosen as model cell lines. Prior to the study, the potential toxicity of **DCM-Cl-CE** was evaluated by a standard counting kit-8, and high biocompatibility could be observed for HepG2 and LO2 cells even as the concentration of **DCM-Cl-CE** reached 100 μM (Figure S23). The activity of CE in HepG2 and LO2 cells was compared under the same conditions for demonstrating whether CE activity is overexpressed in the human liver cancer cells. As shown in Figure 3A, time-dependent experiments showed that after incubation of **DCM-Cl-CE** with cells, the fluorescence intensity in HepG2 cells gradually increased, while almost no fluorescence could be observed in LO2 cells (Figure 3B), indicating that the CE level in HepG2 cells may be higher than that in LO2 cells. The analysis of CE level by a commercial kit further demonstrated that the CE level was higher in HepG2 cells than in LO2 cells (Figure 3C), implying that CE is overexpressed in HepG2 cells,[16] and may be a potential biomarker for indicating the condition of liver

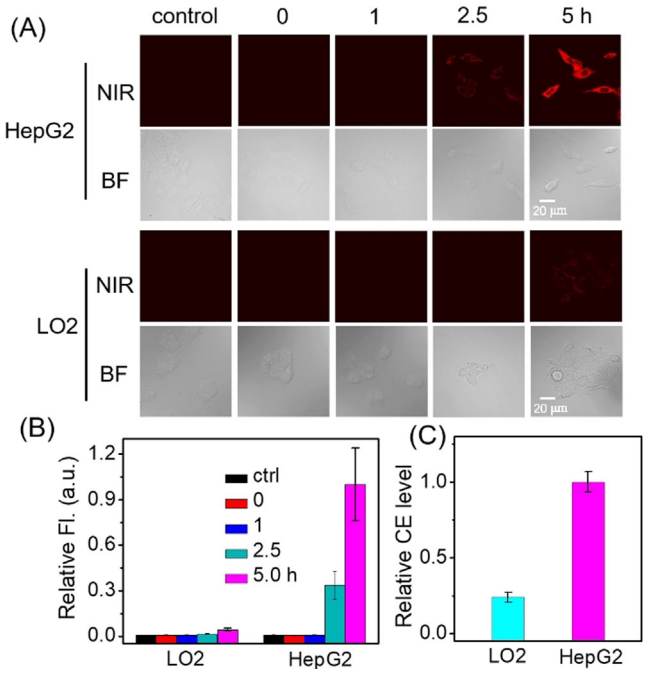

Figure 3. Comparison of CE levels in human liver cancer cells (HepG2 cells) and human normal liver cells (LO2 cells). A) One-photon fluorescence imaging of **DCM-Cl-CE** in HepG2 and LO2 cells at different time points (0, 1, 2.5 and 5 h). The control group: fluorescence imaging of cells without probe. NIR: near-infrared emission channel; BF: bright field channel. B) Relative fluorescence intensity in panel (A). C) Analyses of CE levels by commercial kit in HepG2 and LO2 cells. (λ_{ex} = 540 nm and λ_{em} = 650–750 nm). Scale bar = 20 μm.

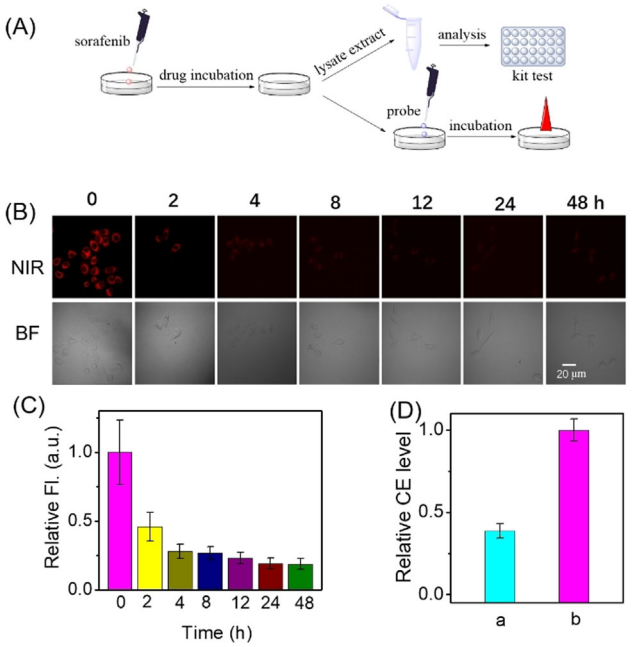

Figure 4. Visualization of CE activity in HepG2 cells treated with an anti-liver-cancer drug (sorafenib) using TP fluorescence imaging. A) Schematic illustration of **DCM-Cl-CE** imaging CE activity in HepG2 cells treated with sorafenib and lysate extraction for analysis of CE levels. B) TP confocal fluorescence imaging for CE activity in HepG2 cells after treatment with sorafenib (10 μM) for different times (0, 2, 4, 8, 12, 24 and 48 h) and then incubation with **DCM-Cl-CE**. C) Relative fluorescence intensity in panel (B). D) Analyses of CE levels in HepG2 cells with (a) sorafenib for 12 h or without (b) sorafenib via a commercial kit. λ_{ex} = 830 nm and λ_{em} = 650–750 nm. Scale bar = 20 μm.

cancer.[5c,d] Two-photon fluorescence for imaging CE activity in HepG2 cells could also be successfully observed (Figure S24).

To further investigate the applicability of **DCM-Cl-CE** in the field of drug development, an inhibitory experiment was implemented in HepG2 and LO2 cells. Compared to that in HepG2 cells and LO2 pretreated with only **DCM-Cl-CE**, the fluorescence intensity in HepG2 and LO2 cells pre-treated with BNPP and then **DCM-Cl-CE** significantly decreased, indicating that the fluorescence intensity indeed arose from the reaction of **DCM-Cl-CE** and CE (Figures S25 and S26).

Discovery of the Effect of Anti-liver-cancer Drug on CE Activity in Hepatocellular Carcinoma Cells

Encouraged by the excellent performance of **DCM-Cl-CE** imaging the overexpression of CE activity in HepG2 cells, we will next evaluate the effect of the anti-liver-cancer drug on CE activity in HepG2 cells with **DCM-Cl-CE**. An anticancer drug (sorafenib) approved for the treatment of liver cancer was employed.[17] As shown in Figure 4, HepG2 cells were divided into seven groups treated with sorafenib for different time points (0, 2, 4, 8, 12, 24 and 48 h), and then incubated with **DCM-Cl-CE** for 5 h. The fluorescence intensity in the cells without sorafenib treatment was used as a control (0 h). With prolonged time, we found that the fluorescence intensity dramatically decreased (Figures 4B, C and S27), indicating that the CE level also decreased, which is further evidenced by analysis of the relative CE level (Figure 4D). These results proved that **DCM-Cl-CE** has the capacity to selectively monitor the change of CE activity and image the different conditions of liver cancer cells during the anticancer drug activation process.

Discovery of DCM-Cl-CE Imaging CE Activity in the Orthotopic Liver Tumor during Treatment of Anticancer Drug

Motivated by the performance of **DCM-Cl-CE** in liver cancer cells, we used this probe to explore the therapeutic effect of an anti-liver-cancer drug (sorafenib) on orthotopic HCC and whether **DCM-Cl-CE** could indicate the in vivo therapeutic condition of mice. We first observed the fluorescence change of **DCM-Cl-CE** in tumor over time. **DCM-Cl-CE** was administered to the subcutaneous HepG2-xenografted tumor-bearing mouse model by intratumoral injection and scanned at different time points (0, 0.5, 1.5, 2.5 and 5 h) using in vivo imaging system. As shown in Figure 5A, obvious fluorescence enhancement could be observed after 5 h, indicating that **DCM-Cl-CE** could successfully image CE activity in the liver tumor in vivo. To further reflect the condition of real liver cancer and evaluate the drug treatment, orthotopic liver cancer model was established at the original hepatic organ. The mice with orthotopic liver cancer were

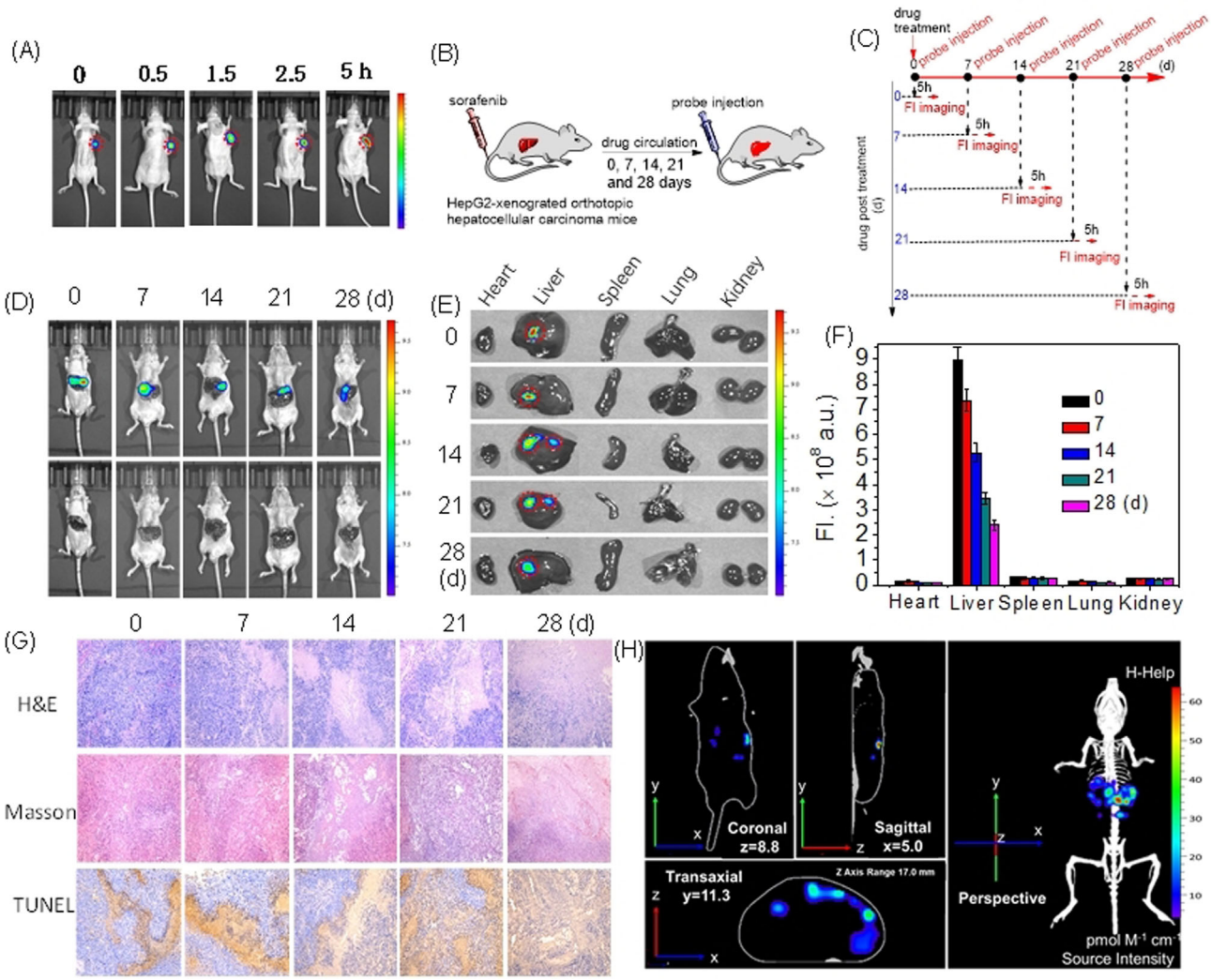

Figure 5. Visualization of imaging the conditions at the orthotopic liver cancer mouse model treated with the anti-liver cancer drug. A) Time-dependent fluorescence imaging of CE activity in the subcutaneous HepG2-xenografted tumor-bearing mouse model was obtained at different time points (0, 0.5, 1.5, 2.5 and 5 h) by intratumoral injection of **DCM-Cl-CE** (10 μM). Red dotted circles indicate the tumor site. B) Schematic illustration of **DCM-Cl-CE** imaging CE activity in the mouse treated with anticancer drug (sorafenib). C) Timeline for the development of mouse model treated with sorafenib and bimodal imaging. D) Imaging CE activity in orthotopic tumor-bearing mice treated with sorafenib by intravenous injection for different times (0, 7, 14, 21 and 28 days), followed by intravenous injection of **DCM-Cl-CE** (10 μM, 100 μL). E) 2D ex vivo imaging of CE in separated organs (heart, liver, spleen, lung, and kidney) sacrificed from mice in panel (D). Red dotted circles indicate the tumor site. F) Fluorescence intensity of the images in the panel (E). G) Hematoxylin and eosin (H&E) staining of orthotopic liver tumor tissue; Masson's staining of orthotopic liver tumor tissues; regional terminal deoxynucleotidyl transferase dUTP nick end labeling (TUNEL) staining of orthotopic liver tumor tissues. H) 3D in vivo imaging of CE activity in the orthotopic liver cancer mouse model pretreated with sorafenib for 0 day, and then treated with **DCM-Cl-CE** (10 μM, 100 μL) for 5 h by intravenous injection. 3D reconstruction of fluorescence molecular tomographic (FMT) imaging of CE activity from coronal, sagittal, and transverse views. (λ_{ex} = 540 nm and λ_{em} = 650–750 nm).

separated into five groups, and then pretreated with an anticancer drug (sorafenib) by intravenous injection for different periods (0, 7, 14, 21 and 28 days). Afterwards, **DCM-Cl-CE** by intravenous injection was incubated with each group for 5 h and then imaged with the imaging system (Figures 5 B and C). As shown in Figure 5 D, compared to the control group (0 day), the fluorescence intensity gradually decreased with prolonged time, indicating that CE activity also decreased. This phenomenon was fully consistent with the fluorescence change in HepG2 cells treated with sorafenib and the analysis of the relative CE activity (Figures 4 B–D). Meanwhile, it also indicated that **DCM-Cl-CE** could selectively image the biomarker (i.e., CE) of liver cancer at the original liver. Besides, based on the higher CE level and selective imaging capacity of **DCM-Cl-CE** in HepG2 cells in Figure 3, it is reasonable to speculate that the fluorescence intensity in the liver tumor may be higher than that in the normal liver region, and thus fluorescence regions may be tumor site in the two-dimensional (2D) ex vivo imaging of the separated organs, indicating that probe bears targeting ability to liver tumor (Figures 5 E and F). To further confirm tumor-targeting ability of probe and treating effect of sorafenib, various staining methods have been performed to illustrate the pathological morphology of the tissues from the fluorescent regions in the liver.

As shown in Figures 5G and S28, the tissue slices in the control group (0 day) were mainly composed of tumor cells. The tumor tissues were less interstitial, and the tumor cells were uniform and tightly distributed. Compared to the control group, the tumor tissue in the treatment group was relatively loose with flaky cell necrosis or apoptosis, and as the time increased, the area of necrosis increased, demonstrating that the tumor-targeting ability of **DCM-Cl-CE** and anticancer drug has some therapeutic effect on the liver cancer. Importantly, from the analysis of above data, we can find that with drug post-treated days (i.e., mice under different conditions), the fluorescence intensity of **DCM-Cl-CE** imaging CE at hepatic organ decreased, accompanied by continuous tumor apoptosis, and a positive correlation between fluorescence change and tumor apoptosis may be established. These data fully indicated that probe has an excellent capacity to target orthotopic liver tumors, and imaging different conditions of liver cancer and elevating the drug treatment of HCC.

Moreover, 3D imaging is a powerful tool for clearly accurate disease diagnosis, especially for uncertain lesions with high spatiotemporal precision.[18] To improve the observation of the CE distribution in deep hepatoma tissue, we carried out a 3D fluorescence molecular tomography (3D FMT) imaging technique based on accurate reconstruction of the in vivo fluorescence distribution. The 3D FMT fluorescence imaging of the orthotopic hepatoma mice was reconstructed through diffuse tomographic algorithms and the CE locations and lesions in the hepatoma were also clearly shown from coronal, sagittal, and transverse views with NIR light-up fluorescence signals (Figures 5H and S29–S32). For the first time, we exemplify in situ 3D fluorescence imaging to clearly visualize the CE activity in tumors. This could be provided as an important tool for the imaging-guided diagnosis and surgical resection of HCC.

Conclusion

In summary, we have proposed dimethyl carbamate as a specific recognition moiety for CE activity, which was combined with a substituted self-immolative linker to develop a series of compounds (**P1**–**P8**) for screening the best substrate for CE activity. Based on the best recognition moiety of **P3**, a NIR TP fluorogenic probe (**DCM-Cl-CE**) was prepared for in vivo imaging of CE activity that can also effectively eliminate the interference from other hydrolyses. This probe displayed high sensitivity, selectivity, stability, and pH independence. Importantly, this probe has proven to image the difference in CE activity between HepG2 and LO2 cells, and successfully monitor changes in CE activity in HepG2 cells treated with anticancer drugs, making it applicable to indicate for the evaluation of drug treatment of HCC in vivo. With condition changing at different time points post-treatment in the mice model bearing orthotopic liver tumor (i.e., mice under different conditions), a positive correlation may be established between the fluorescence intensity of **DCM-Cl-CE** in vivo and continuous tumor apoptosis, indicating **DCM-Cl-CE** can be used to evaluate the condition of HCC chemotherapy. Moreover, for the first time, the CE activity in the tumor site with a high-resolution 3D view was visualized, allowing for possible image-guided diagnosis and surgical resection of HCC in the future. Considering the high selectivity and sensitivity, stabilities, and biocompatibility, we believe this enzyme-activated NIR TP fluorescent probe will be provided as an effective tool for in vivo and in situ monitoring the condition of the liver cancer and evaluations of drug treatments.

Acknowledgements

J.Y. thanks the National Research Foundation of Korea (NRF), which was funded by the Korea government (MSIP) (No. 2012R1A3A2048814). F.Y. thanks National Natural Science Foundation of China (Nos. 21864011 and 21775162), Hainan Key Research and Development Project (Grant ZDYF2020133).

Conflict of interest

The authors declare no conflict of interest.

Stichwörter: activatable probes · analytical methods · fluorogenic imaging · orthotopic hepatocellular carcinoma · specific substrates

[1] a) X. Li, X. Gao, W. Shi, H. Ma, *Chem. Rev.* **2014**, *114*, 590 – 659; b) H. W. Liu, L. Chan, C. Xu, Z. Li, H. Zhang, X. B. Zhang, W. H. Tan, *Chem. Soc. Rev.* **2018**, *47*, 7140 – 7180; c) K. J. Bruemmer, S. W. M. Crossley, C. J. Chang, *Angew. Chem. Int. Ed.* **2020**, *59*, 13734 – 13762; *Angew. Chem.* **2020**, *132*, 13838 – 13867; d) L. Wang, M. Tran, E. D'Este, J. Roberti, B. Koch, L. Xue, K. Johnsson, *Nat. Chem.* **2020**, *12*, 165 – 172; e) S. H. Gardner, C. J. Reinhardt, J. Chan, *Angew. Chem. Int. Ed.* **2021**, *60*, 5000 – 5009; *Angew. Chem.* **2021**, *133*, 5052 – 5062; f) J. Zhang, X. Chai, X. P. He, H. J. Kim, J. Yoon, H. Tian, *Chem. Soc. Rev.* **2019**, *48*, 683 – 722; g) L. Wang, J. Hiblot, C. Popp, L. Xue, K. Johnsson, *Angew. Chem. Int. Ed.* **2020**, *59*, 21880 – 21884; *Angew. Chem.* **2020**, *132*, 22064 – 22068; h) L. Wang, M. S. Frei, A. Salim, K. Johnsson, *J. Am. Chem. Soc.* **2019**, *141*, 2770 – 2781; i) R. Obara, M. Kamiya, Y. Tanaka, A. Abe, R. Kojima, T. Kawaguchi, M. Sugawara, A. Takahashi, T. Noda, Y. Urano, *Angew. Chem. Int. Ed.* **2021**, *60*, 2125 – 2129; *Angew. Chem.* **2021**, *133*, 2153 – 2157.

[2] a) Q. Miao, D. C. Yeo, C. Wiraja, J. Zhang, X. Ning, C. Xu, K. Pu, *Angew. Chem. Int. Ed.* **2018**, *57*, 1256 – 1260; *Angew. Chem.* **2018**, *130*, 1270 – 1274; b) D. Zhang, L. Wang, X. Yuan, Y. Gong, H. Liu, J. Zhang, X. Zhang, Y. Liu, W. Tan, *Angew. Chem. Int. Ed.* **2020**, *59*, 695 – 699; *Angew. Chem.* **2020**, *132*, 705 – 709; c) L. Yuan, W. Lin, K. Zheng, L. He, W. Huang, L. Silman, J. Sussman, *Chem. Soc. Rev.* **2013**, *42*, 622 – 661; d) Z. Guo, C. Yan, W. H. Zhu, *Angew. Chem. Int. Ed.* **2020**, *59*, 9812 – 9825; *Angew. Chem.* **2020**, *132*, 9896 – 9909; e) N. Karton-Lifshin, E. Segal, L. Omer, M. Portnoy, R. Satchi-Fainaro, D. Shabat, *J. Am. Chem. Soc.* **2011**, *133*, 10960 – 10965; f) Z. Guo, S. Park, J. Yoon, I. Shin, *Chem. Soc. Rev.* **2014**, *43*, 16 – 29; g) H. M. Kim, B. R. Cho, *Acc. Chem. Res.* **2009**, *42*, 863 – 872; h) D. Kim, H. G. Ryu, K. H. Ahn, *Org. Biomol. Chem.* **2014**, *12*, 4550 – 4556; i) Y. W. Jun, T. Wang, S. Hwang, D. Kim, D. Ma, K. H. Kim, S. Kim, J. Jung, K. H. Ahn, *Angew. Chem. Int. Ed.* **2018**, *57*, 10142 – 10147; *Angew. Chem.*

2018, *130*, 10299 – 10304; j) J. Ning, W. Wang, G. Ge, P. Chu, F. Long, Y. Yang, Y. Peng, L. Fei, X. Ma, T. D. James, *Angew. Chem. Int. Ed.* **2019**, *58*, 9959 – 9963; *Angew. Chem.* **2019**, *131*, 10064 – 10068.

[3] a) J. Balogh, D. Victor, E. H. Asham, S. G. Burroughs, M. Boktour, A. Saharial, X. Li, R. M. Ghobrial, Jr., H. P. Monsour, *J. Hepatocell. Carcinoma* **2016**, *3*, 41 – 53; b) J. Bruix, L. Boix, M. Sala, J. M. Llovet, *Cancer Cell* **2004**, *5*, 215 – 219; c) X. W. Wang, S. P. Hussain, T. I. Huo, C. G. Wu, M. Forgues, L. J. Hofseth, C. Brechot, C. C. Harris, *Toxicology* **2002**, *181*, 43 – 47.

[4] a) M. Upender, S. Rashmi-Gopal, S. Sudhir, *Drug Discovery Today* **2005**, *10*, 965 – 972; b) S. Dasari, R. Wudayagiri, L. Valluru, *Clin. Chim. Acta* **2015**, *445*, 7 – 11.

[5] a) P. Reichl, W. Mikulits, *Oncol. Rep.* **2016**, *36*, 613 – 625; b) K. Na, E. Y. Lee, H. J. Lee, K. Y. Kim, H. Lee, S. K. Joeng, A. S. Jeong, S. Y. Cho, S. A. Kim, S. Y. Song, K. S. Kim, S. W. Cho, H. Kim, Y. K. Paik, *Proteomics* **2009**, *9*, 3989 – 3999; c) P. Chen, W. Kuang, Z. Zhen, S. Yang, Y. Liu, L. Su, K. Zhao, G. Liang, *Theranostics* **2019**, *9*, 7359 – 7369; d) X. Lv, D. Wang, L. Feng, P. Wang, L. W. Zou, D. C. Hao, J. Hou, J. N. Cui, L. Yang, *RSC Adv.* **2016**, *6*, 4302 – 4309; e) K. Na, S. K. Jeong, M. Lee, S. Cho, S. Kim, M. J. Lee, H. Kim, K. Kim, H. Wong, Y. K. Paik, *Int. J. Cancer* **2013**, *133*, 408 – 416.

[6] a) J. Li, M. A. Baird, W. Tai, L. S. Zweifel, K. M. A. Waldorf, Jr., N. Gale, L. Rajagopal, R. H. Pierce, X. Gao, *Nat. Biomed. Eng.* **2017**, *1*, 0082; b) Y. Wu, S. Huang, J. Wang, L. Sun, F. Zeng, S. Zhu, *Nat. Commun.* **2018**, *9*, 3983.

[7] a) X. Wu, W. Shi, X. Li, H. Ma, *Acc. Chem. Res.* **2019**, *52*, 1892 – 1902; b) Y. L. Qi, L. Guo, L. L. Chen, H. Li, Y. S. Yang, A. Q. Jiang, H. L. Zhu, *Coord. Chem. Rev.* **2020**, *421*, 213460.

[8] a) Y. Zhang, W. Chen, D. Feng, W. Shi, X. Li, H. Ma, *Analyst* **2012**, *137*, 716 – 721; b) J. Chen, D. Liao, Y. Wang, H. Zhou, W. Li, C. Yu, *Org. Lett.* **2013**, *15*, 2132 – 2135; c) S. Yoo, M. S. Han, *Chem. Commun.* **2019**, *55*, 14574 – 14577; d) S. Y. Liu, H. Xiao, J. Q. Yang, S. H. Yang, Y. Li, W. C. Yang, G. F. Yang, *ACS Sens.* **2018**, *3*, 2118 – 2128.

[9] M. Pohanka, *Int. J. Mol. Sci.* **2014**, *15*, 9809 – 9825.

[10] a) M. K. Danks, C. L. Morton, E. J. Krull, P. J. Cheshire, L. B. Richmond, C. W. Naeve, C. A. Pawlik, P. J. Houghton, P. M. Potter, *Clin. Cancer Res.* **1999**, *5*, 917 – 924; b) D. Oosterhoff, H. Pinedo, I. H. Van der Meulen, M. De Graaf, T. Sone, F. Kruyt, V. Van Beusechem, H. Haisma, W. Gerritsen, *Br. J. Cancer* **2002**, *87*, 659 – 664; c) D. J. Burkhart, B. L. Barthel, G. C. Post, B. T. Kalet, J. W. Nafie, R. K. Shoemarker, T. H. Koch, *J. Med. Chem.* **2006**, *49*, 7002 – 7012.

[11] a) J. Yan, S. Lee, A. Zhang, J. Yoon, *Chem. Soc. Rev.* **2018**, *47*, 6900 – 6916; b) J. Ning, T. Liu, P. Dong, P. Wang, W. Wang, G. Ge, B. Wang, Z. Yu, L. Shi, X. Tian, X. Huo, L. Feng, C. Wang, C. Sun, J. Cui, T. D. James, X. Ma, *J. Am. Chem. Soc.* **2019**, *141*, 1126 – 1134.

[12] X. Wu, W. Shi, X. Li, H. Ma, *Angew. Chem. Int. Ed.* **2017**, *56*, 15319 – 15323; *Angew. Chem.* **2017**, *129*, 15521 – 15525.

[13] a) K. Gu, Y. Xu, H. Li, Z. Guo, S. Zhu, S. Zhu, P. Shi, T. D. James, H. Tian, W. H. Zhu, *J. Am. Chem. Soc.* **2016**, *138*, 5354 – 5358; b) K. Gu, W. Qiu, Z. Guo, C. Yan, S. Zhu, D. Yao, P. Shi, H. Tian, W. H. Zhu, *Chem. Sci.* **2019**, *10*, 398 – 405; c) W. Wu, W. Sun, Z. Guo, J. Tang, Y. Shen, T. D. James, H. Tian, W. H. Zhu, *J. Am. Chem. Soc.* **2014**, *136*, 3579 – 3588.

[14] a) H. Eng, M. Niosi, T. S. Mcdonald, A. Wolford, Y. Chen, S. T. M. Simila, J. N. Bauman, J. Warmus, A. S. Kalgutkar, *Xenobiotica* **2010**, *40*, 369 – 380; b) M. J. Hatfield, P. M. Potter, *Expert Opin. Ther. Pat.* **2011**, *21*, 1159 – 1171.

[15] J. A. Carr, D. Franke, J. R. Caram, C. F. Perkinson, M. Saif, V. Askoxylakis, M. Datta, D. Fukumura, R. K. Jain, M. G. Bawendi, O. T. Brun, *Proc. Natl. Acad. Sci. USA* **2018**, *115*, 4465 – 4470.

[16] J. Li, J. Shi, J. E. Medina, J. Zhou, X. Du, H. Wang, C. Yang, J. Liu, Z. Yang, D. M. Dinulescu, B. Xu, *Adv. Healthcare Mater.* **2017**, *6*, 1601400.

[17] a) J. M. Llovet, S. Ricci, V. Mazzaferro, P. Hilgard, E. Gane, J. F. Blanc, A. C. de Oliveria, A. Santoro, J. L. Raoul, A. Forner, M. Schwartz, C. Porta, S. Zeuzem, L. Bolondi, T. F. Greten, P. R. Falle, J. F. Seitz, I. Borbath, D. Haussinger, T. Giannaris, M. Shan, M. Moscovici, D. Voliotis, J. Bruix, *N. Engl. J. Med.* **2008**, *359*, 378 – 390; b) M. Kudo, R. S. Finn, S. Qin, K. H. Han, K. Ikeda, F. Piscaglia, A. Baron, J. W. Park, G. Han, J. Jassem, J. F. Blanc, A. Vogel, D. Komov, T. R. Evans, C. Lopez, C. Dutcus, M. Guo, K. Saito, S. Kraljevic, T. Tamai, M. Ren, A. L. Cheng, *Lancet* **2018**, *391*, 1163 – 1173.

[18] a) V. Ntziachristos, C. Bremer, E. E. Graves, J. Ripoll, R. Weissleder, *Mol. Imaging* **2002**, *1*, 82 – 88; b) E. E. Graves, R. Weissleder, V. Ntziachristos, *Curr. Mol. Med.* **2004**, *4*, 419 – 430.

Manuskript erhalten: 25. Januar 2021
Veränderte Fassung erhalten: 8. April 2021
Akzeptierte Fassung online: 3. Mai 2021
Endgültige Fassung online: ■■. ■■ ■■■■

Forschungsartikel

Fluorescent Probes

X. Wu, R. Wang, S. Qi, N. Kwon, J. Han, H. Kim, H. Li, F. Yu,* J. Yoon* ——— ▮▮▮▮–▮▮▮▮

Rational Design of a Highly Selective Near-Infrared Two-Photon Fluorogenic Probe for Imaging Orthotopic Hepatocellular Carcinoma Chemotherapy

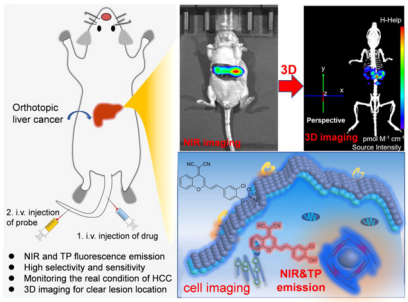

In this report, we show that a carbamate as recognition unit has an excellent selectivity for a hepatocellular carcinoma chemotherapy (HCC)-related biomarker (carboxylesterase, CE) without interference from other hydrolases. We developed a near-infrared two-photon fluorescent probe with high selectivity and strong fluorescence signals towards CE activity, enabling it to successfully monitor CE activity for evaluating HCC chemotherapy in vivo.

↖↖ These are not the final page numbers!